IEEE Photonics Journal
An IEEE Photonics Society Publication

Open Access

Sand-Dust Image Restoration Based on Reversing the Blue Channel Prior

Volume 12, Number 2, April 2020

GuXue Gao
HuiCheng Lai
ZhenHong Jia
YueQin Liu
YaLi Wang

DOI: 10.1109/JPHOT.2020.2975833

IEEE photonics SOCIETY
IEEE

Sand-Dust Image Restoration Based on Reversing the Blue Channel Prior

GuXue Gao, HuiCheng Lai, ZhenHong Jia, YueQin Liu, and YaLi Wang

College of Information Science and Engineering, Xinjiang University, Urumqi 830046, China

DOI:10.1109/JPHOT.2020.2975833

Manuscript received January 31, 2020; accepted February 18, 2020. Date of publication February 24, 2020; date of current version March 13, 2020. This work was supported by the National Natural Science Foundation of China (NSFC) under Grants #61561048 and #U1803261. Corresponding author: HuiCheng Lai (e-mail: 2235108241@qq.com).
This article has supplementary downloadable material available at http://ieeexplore.ieee.org, provided by the authors.

Abstract: Images acquired under sand-dust weather conditions are severely degraded, with low contrast and severe color shift. The reason is that, due to the influence of sand-dust particles, light is scattered and absorbed, resulting in a blurred image and low contrast; the color shift is caused by the rapid attenuation of blue light. Therefore, to solve the problem of color shift and poor visibility in sand-dust images, this paper proposes a sand-dust image restoration method based on reversing the blue channel prior (RBCP). Under the influence of the blue channel, the dark channel prior (DCP) method will fail. Therefore, the method first reverses the blue channel of the sand-dust image and uses the dark channel prior method, which we call RBCP, and then, RBCP is used to estimate the atmospheric light and transmission map and recover the sand-dust image. The restored image shows significantly improved visibility. When estimating the transmission map, a guiding filter is used to improve the coarse transmission map, and a tolerance mechanism is introduced to modify the transmission map of bright areas in the sky to solve the problem of distortion in the sky. Finally, combined with the gray world, an adaptive color adjustment factor is introduced into the restoration model to remove the color shift. Experimental results via qualitative and quantitative evaluation demonstrate that the proposed method can effectively recover clear sand-dust images and produce results superior to those of other state-of-the-art methods.

Index Terms: Color shift, sand-dust image, RBCP, tolerance mechanism.

1. Introduction

Most outdoor vision applications, such as intelligent surveillance [1], autonomous navigation [2], and vehicle tracking and monitoring systems [3], require clear visibility of the input image. However, in inclement sand-dust weather conditions, the contrast and color of the image are greatly reduced, which seriously affects the quality of the image, resulting in various vision systems failing to work properly. Therefore, it is of great practical significance to study visibility enhancement algorithms of sand-dust degradation images, remove the influence of sand-dust weather from images, and expand the application range of these vision systems to ensure more reliable operation. Visibility enhancement technology for sand-dust degradation images is also an important part of the image video processing and computer vision fields, and this research subject has wide application prospects.

In sand-dust weather, because the diameter of dust particles is longer than the wavelength of visible light, under the influence of Mai scattering [4], blue light is scattered and absorbed in large quantities, which causes an image acquired in sand-dust weather conditions to show the problems of overall yellowing, low contrast, color shift and distortion. The main problems of sand-dust images are color shift and haze removal. The classic color correction methods are [5], [6], which were developed recently by new color correction methods [7]–[9]. Liu *et al.* [7] proposed a method to detect and remove color shifts, but this method is not suitable for sand-dust images. [8]'s method achieved color correction through the halftone method, but it did not work well on sand-dust images with yellow tones. Afifi *et al.* [9] introduced the k-nearest-neighbor algorithm to calculate a color mapping function to correct the color of images that cannot be processed by white balancing. This algorithm can effectively process images that white balancing cannot process. The color shift of the sand-dust image is corrected to a certain degree. Since a sand-dust image is greatly different from a constructed image, the corrected sand-dust image will have the problem of color distortion. At present, haze removal algorithms fall into two categories: one category is image enhancement processing algorithms, which focus on improving the contrast of an image and highlighting the details in the image but loses some information on prominent details; the other category is image restoration algorithms based on an atmospheric scattering model. This kind of restoration algorithm removes fog from the physical causes of haze, and the defogging effect is relatively good. The classical algorithms include [10]–[14], and a series of defogging algorithms were developed based on the dark channel proposed by He *et al.* [14]. Currently, the more popular methods are learning-based image restoration methods [15]–[18]. This kind of algorithm extracts the haze feature map and uses a deep neural network to learn the transmittance and atmospheric light to recover the haze-free image with good effect. However, the image defogging algorithm is not very suitable for sand removal. Compared with a hazy image, not only does a sand-dust image have a serious color shift but also sand-dust particles have a larger radius than haze [19], and the absorption and scattering of light is stronger, making the clarity of sand-dust images worse. Therefore, restoring sand-dust images is still a very challenging task.

However, the research results of visibility restoration on sand-dust degraded images are few, and there are still many problems in existing algorithms, such as color shift and insufficient contrast. Sand-dust image removal algorithms can be divided into two categories: image enhancement and image restoration. From the perspective of image enhancement, Yan *et al.* [20] proposed a sand-dust image enhancement algorithm based on the POSHE algorithm. The algorithm uses global PAL to process the R, G and B channels to change the histogram distribution to achieve color correction, but it is prone to color distortion; it uses POSHE to enhance image contrast. Although the contrast of sand-dust images is improved, the enhancement effect of prospective images is not good. Fu *et al.* [19] proposed a fusion-based algorithm to overcome the problems of sand-dust degraded images, used a statistical strategy to correct the color shift of sand-dust degraded images, and then fused input graphs with different brightness and weight graphs to obtain enhanced images. Through this algorithm, the color of a sand-dust degraded image is corrected, and the contrast is improved, but the overall image is dark. From the perspective of image restoration, Yu *et al.* [21] proposed a single sand-dust degraded image restoration algorithm based on an atmospheric scattering model and information loss constraint, which can improve the contrast of different kinds of sand-dust degraded images. This method accurately estimates the atmospheric light by iterating atmospheric light to compensate for the color shift and achieve color fidelity; however, this brings the problem of halos. Peng *et al.* [22], [23] proposed a method of scene light difference to estimate the transmission image, which can improve the contrast of an image, and scaled each color channel to remove color shift through an adaptive color adjustment factor, but this method cannot effectively solve the problem of color deviation. Huang *et al.* [24] modified the transmission map by means of median filtering and gamma correction and used a color channel difference method to correct color shift. The effect of color correction was not ideal, and a blueness phenomenon appeared in the sky area. Huang *et al.* [25], [26] removed sand dust based on the dark channel prior method to improve contrast. In terms of color correction, [26] realized color correction through the CA model, but bluishness and color distortion occurred. [25] established a Laplacian distribution for

the R, G, and B channels to achieve color correction, effectively removing color shift. Ren *et al.* [27] proposed an algorithm consisting of a coarse-scale net that predicts a holistic transmission map based on an entire image and a fine-scale net that refines results locally. This method can effectively improve the sharpness of a sand-dust image but cannot solve the color shift problem. Shin *et al.* [28] presented a novel optimization-based dehazing algorithm that combines radiance and reflectance components with an additional refinement using a structure-guided ℓ_0 -norm filter. The method improves the visibility of sand-dust images, but the effect of color correction is not ideal. Shi *et al.* [29] proposed a dark channel sand-dust enhancement method based on halo elimination. First, the color component AB was used to remove the color shift in the LAB color space, and then the improved dark channel was used to remove haze in the RGB space. Finally, in the conversion to the LAB space, the brightness L is stretched to enhance contrast. This method effectively improves the visibility of the image, but the recovered colors are dim. Ren *et al.* [30] proposed a gated fusion network to remove haze. This method relies on an end-to-end training network, uses contrast enhancement and gamma correction to remove haze, uses white balance to remove color shift, and then uses the weight map obtained by the network to obtain the final image. This method can effectively improve the contrast of sand-dust images, and it can better enhance perspective; however, it cannot effectively remove color shift.

To solve the problem of color shift and low contrast of sand-dust images, based on DCP, this paper proposes a sand-dust image restoration method based on reversing the blue channel prior. The method uses RBCP to estimate the atmospheric light and transmission map, refines the transmission map by guiding filtering, and then introduces a tolerance mechanism to improve the transmission map in the sky to repair the color distortion of the sky. Finally, combined with the gray world, an adaptive color adjustment factor is introduced to remove color shift in the atmospheric scattering model. The following are the key features of our proposed method.

1) RBCP is proposed based on DCP, and the atmospheric light and transmission map are estimated based on this.
2) A tolerance mechanism is introduced to repair the transmission map of bright areas in the sky to avoid distortion in the sky.
3) Based on the gray world, the color correction factor is introduced into the atmospheric scattering model, which removes the color shift well.

The structure of our paper is as follows: In Section 2, we introduce the image restoration model based on the DCP. Section 3 presents the details of our method. Section 4 presents the experimental results of qualitative and quantitative analysis of the proposed method and the other state-of-the-art methods. Finally, the conclusion is presented in Section 5.

2. Restoration Based on DCP

The dark channel prior haze removal algorithm is a restoration algorithm based on the atmospheric scattering model. The model describes the formation process of fog images. Its formula is as follows:

$$I(x) = J(x)t(x) + A(x)(1 - t(x)) \tag{1}$$

where $I(x)$ is the intensity of the observed hazy image, $J(x)$ represents the scene radiance of the ideal haze-free image, A represents the atmospheric light, and $t(x)$ represents the transmission map describing the portion of the light that arrives at the digital camera without scattering. Generally, the homogenous atmosphere can be assumed to be uniform, and the scene radiance is exponentially attenuated according to the depth of the scene. The transmission map can be expressed as:

$$t(x) = e^{-\beta d(x)} \tag{2}$$

where β is the scattering coefficient of the atmosphere and $d(x)$ is the scene depth between the digital camera and the captured object for each pixel x in the image. He *et al.* [14] proposed a dark channel a priori-based defogging algorithm, which assumes that there exists such a statistical rule in outdoor images; that is, in most non-sky local areas, at least one channel of certain pixels will

(a) (b) (c)

Fig. 1. DCP defogging results. (a) Hazy image. (b) Dark channel. (c) Dehazed result.

have a very low value, i.e., it will be a dark channel. The dark channel of an image is described by the following formula:

$$J^{\text{dark}}(x) = \min_{c\in\{r,g,b\}} \left(\min_{y\in\Omega(x)} (J^c(y)) \right) \tag{3}$$

where J^c is a color channel of the RGB image J, $\min_{c\in\{r,g,b\}}$ is the minimum value of the color channel, $\Omega(x)$ is a local patch centered at location x, and $\min_{y\in\Omega(x)}$ is a minimum filter. $J^{\text{dark}}(x)$ represents the dark channel of the outdoor haze-free image. As described in [14], if J is an outdoor haze-free image, the corresponding intensity of the dark channel $J^{\text{dark}}(x)$ is low and close to zero.

$$J^{\text{dark}}(x) \to 0 \tag{4}$$

Using this prior and (1), we can obtain the estimated transmission map:

$$t(x) = 1 - w \min_c \left(\min_{y\in\Omega(x)} \left(\frac{I^c(y)}{A^c} \right) \right) \tag{5}$$

where $w = 0.95$ so that some haze is preserved in the restored scene radiance so that the image looks more natural. It is estimated from the above equation that the transmission map is rough. To improve accuracy, He proposed applying a soft mapping algorithm to improve the transmission map. Recalling that the improved transfer map is $t(x)$, then the final restored image $J(x)$ is:

$$J(x) = \frac{I(x) - A(x)}{\max(t(x), t_0)} + A(x) \tag{6}$$

The value of t_0 is assumed to be 0.1, and the value of atmospheric light A is the highest-intensity pixel in the original input image according to its correspondence to the brightest 0.1% of pixels in the dark channel. Fig. 1 shows the effect of the DCP dehazing algorithm and the corresponding dark channel.

For a hazy image, the larger the value of the dark channel is, the larger the corresponding haze concentration. Thus, the dark channel prior can accurately estimate the transmission map and atmospheric light and then use the atmospheric scattering model to recover a clear image.

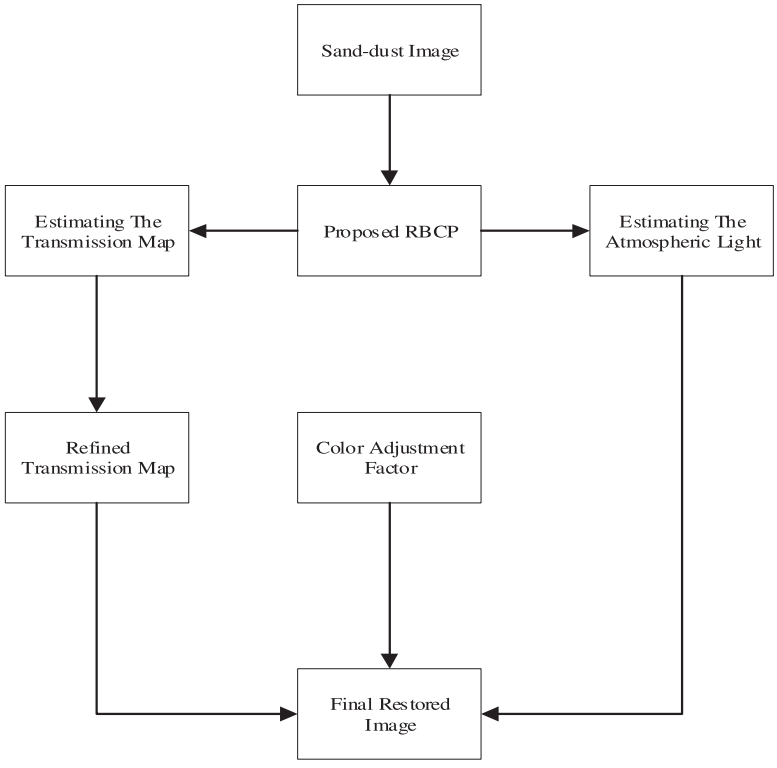

Fig. 2. The flowchart of the proposed algorithm.

3. Details of Our Method

Fig. 2 is the flow chart of the proposed algorithm.

3.1 Reverse the Blue Channel Prior (RBCP)

Because most blue light is scattered and absorbed, which causes the DCP to fail and leads to inaccurate ambient light and transmission estimation [23], the dark channel prior method is not suitable for sand-dust images. According to (2), when the scene depth $d(x) = 0$, $t(x) = 1$. The atmospheric light A has no influence on formula (1), resulting in $I(x) = J(x)$. With increasing scene depth, the transmission gradually decreases to zero, and the contribution of atmospheric light to formula (1) gradually increases until it is close to $I(x)$. As the blue light of the dust image decays faster with increasing distance, the sand-dust image still obeys the above rules, so formula (1) needs to be adjusted:

$$\begin{aligned} 1 - I^B(x) &= t^B(x)(1 - J^B(x)) + (1 - t^B(x))(1 - A^B) \\ I^R(x) &= t^R(x)J^R(x) + (1 - t^R(x))A^R \\ I^G(x) &= t^G(x)J^G(x) + (1 - t^G(x))A^G \end{aligned} \tag{7}$$

(7) still satisfies the gradual attenuation of light as distance increases. Let $I^{B'}(x) = 1 - I^B(x)$, $J^{B'}(x) = 1 - J^B(x)$, $A^{B'} = 1 - A^B$; then:

$$I^{B'}(x) = t^B(x)J^{B'}(x) + (1 - t^B(x))A^{B'} \tag{8}$$

Therefore, (7) can be modified to:

$$I'_\lambda(x) = J'_\lambda(x)t'(x) + (1 - t'_\lambda(x))A'_\lambda \tag{9}$$

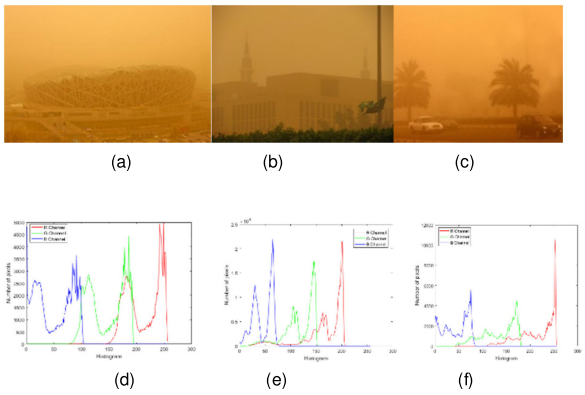

Fig. 3. Sand-dust images and their corresponding color histograms. (a), (b) and (c) are sandstorm images. (d), (e) and (f) are their corresponding color histograms.

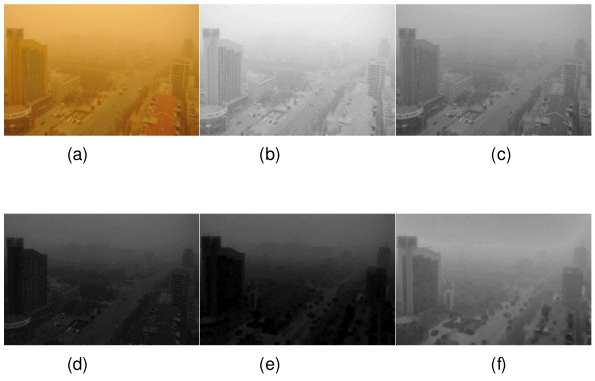

Fig. 4. Effect of the reversed blue channel. (a) Sand-dust image. (b) Red channel. (c) Green channel. (d) Blue channel. (e) Dark channel. (f) The dark channel after reversing the blue channel.

where $I'_\lambda(x)$ is the image after the blue channel is inverted, $J'_\lambda(x)$ is the recovered clear image, and A'_λ is the corresponding atmospheric light intensity. As shown in Fig. 3, the histogram statistics of sand-dust images show that the value of the blue channel decreases faster, which affects the misjudgment of the dark channel a priori value [24]. To reflect this fact, the dark channel prior (2) is modified to:

$$J'_{\text{dark}}(x) = \min\left(\min_{y\in\Omega(x)}(1 - J^B(y)), \min_{y\in\Omega(x)}(J^R(y), \min_{y\in\Omega(x)}(J^G(y))\right) \approx 0 \tag{10}$$

$J'_{\text{dark}}(x)$ reverses the blue channel prior (which we call RBCP). The result of RBCP of the sand-dust image is shown in part (f) of Fig. 4 and Fig. 5. Since the value of the blue channel decays faster, the blue channel is darker, affecting the dark channel and making the dark channel more similar to the blue channel. The RBCP image is more similar to the dark channel in the haze of Fig. 1 and better satisfies the prior rule of the dark channel.

3.2 Guided Filter-Improved Transmission

Minimizing the operation of both sides of (9) and assuming that transmission is constant in the local area, the following can be obtained:

$$t_\lambda(x) = 1 - w\min_{y\in\Omega(x)}\left(\min_{\lambda\in\{R,G,B\}}\left(\frac{I'(y)}{A'_\lambda}\right)\right) \tag{11}$$

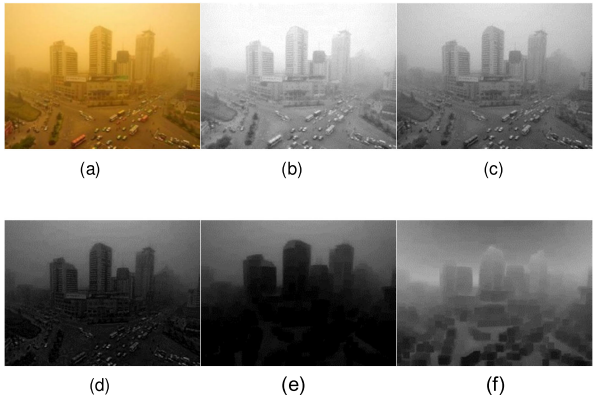

Fig. 5. Effect of the reversed blue channel. (a) Sand-dust image. (b) Red channel. (c) Green channel. (d) Blue channel. (e) Dark channel. (f) The dark channel after reversing the blue channel.

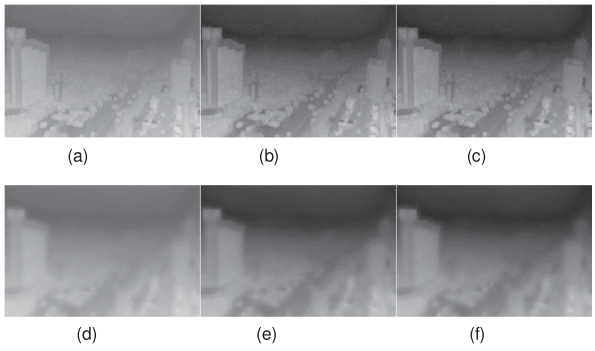

Fig. 6. Refined transmission of Fig. 4(a). (a) Coarse transmission of the R channel. (b) Coarse transmission of the G channel. (c) Coarse transmission of the B channel. (d) Refined transmission of the R channel. (e) Refined transmission of the G channel. (f) Refined transmission of the B channel.

Therefore, the three-channel transmission can be written as:

$$t_R(x) = 1 - \frac{w \min_{y\in\Omega(x)}(\min I'_R(y))}{A'_R}$$

$$t_G(x) = 1 - \frac{w \min_{y\in\Omega(x)}(\min I'_G(y))}{A_G}$$

$$t_B(x) = 1 - \frac{w \min_{y\in\Omega(x)}(\min I'_B(y))}{A_B} \tag{12}$$

$I'_R(y) = I_R(y)$, $I'_G(y) = I_G(y)$, $I'_B(y) = I'_B(y)$, $I_R(y)$, $I_G(y)$ and $I_B(y)$ are the pixel values of the R, G and B channels, respectively. A_R, A_G, and A_B are the atmospheric light values estimated by using the RBCP method proposed in this paper. The method of obtaining atmospheric light is the same as the method of He; the largest pixel point of 0.1% in the $J'_{\text{dark}}(x)$ image is selected, and the largest pixel value in the corresponding haze image is selected as the value of atmospheric light. Since the calculation of the transmission map uses block operations, there are many small blocks in the image, which are relatively rough, so this paper uses a guiding filter [31] to refine the coarse transmission map, as shown in Fig. 6 and Fig. 7.

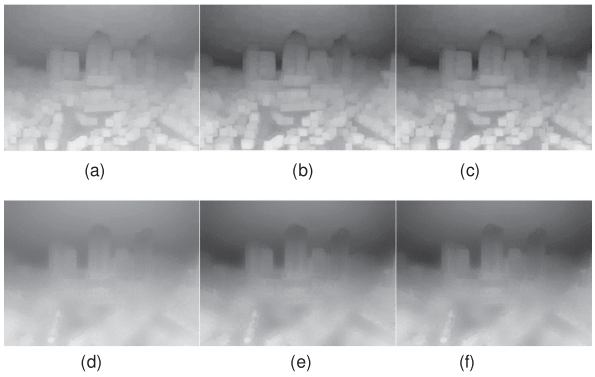

Fig. 7. Refined transmission of Fig. 5(a). (a) Coarse transmission of the R channel. (b) Coarse transmission of the G channel. (c) Coarse transmission of the B channel. (d) Refined transmission of the R channel. (e) Refined transmission of the G channel. (f) Refined transmission of the B channel.

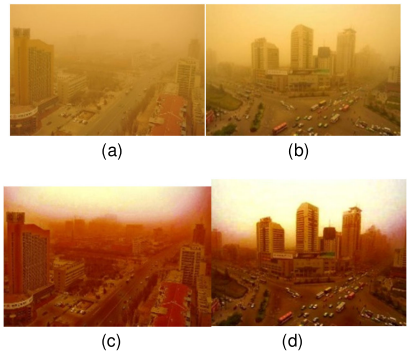

Fig. 8. Results of sand-dust removal. (a) and (b) are sand-dust images. (c) and (d) are the corresponding recovery results.

From Fig. 6 and Fig. 7, we observed that guided filtering improves the coarse transmission map very well.

3.3 Atmospheric Scattering Model Restoration

After calculating the atmospheric light and transmission map, the clear sand-dust image can be restored by (6):

$$J^R(x) = \frac{I^R(x) - A^R}{\max(t^R(x), t_0)} + A^R$$
$$J^G(x) = \frac{I^G(x) - A^G}{\max(t^G(x), t_0)} + A^G$$
$$J^B(x) = \frac{I^B(x) - A^B}{\max(t^B(x), t_0)} + A^B \tag{13}$$

Formula (13) can be written as:

$$J^c_{c\in\{R,G,B\}}(x) = \frac{I^c - A^c}{\max(t^c(x), t_0)} + A^c \tag{14}$$

The recovered sand-dust image is shown in Fig. 8:

(a) (b)

Fig. 9. Resulting images with improved sky area distortion. (a) Recovered image of Fig. 8(c). (b) Recovered image of Fig. 8(d).

As seen from Fig. 8, the contrast and clarity of the image have been effectively improved; however, the sky area is distorted and needs to be improved.

3.4 Restoration Model After Improvement of the Sky Area Transmission Map

If the dark channel assumption is not considered, according to (1) and using the minimum operator, the accurate transmission map is as follows:

$$t_{\text{real}}(x) = \frac{1 - \min_c \left\{ \min_{y \in \Omega(x)} \left(\frac{I^c(y)}{A^c} \right) \right\}}{1 - \min_c \left\{ \min_{y \in \Omega(x)} \left(\frac{J^c(x)}{A^c} \right) \right\}} \tag{15}$$

In bright regions, $\min\limits_c \{\min_{y \in \Omega(x)} (\frac{J^c(x)}{A^c})\}$ cannot be approximated as zero, and the denominator of (15) is less than 1, so the actual transmission $t_{\text{real}}(x)$ is greater than the estimated transmission $t(x)$ of the dark channel. To eliminate color distortion in the sky, the transmission function of the bright area should be adjusted to make the estimated value of $t(x)$ more consistent with $t_{\text{real}}(x)$ without destroying the unified atmospheric scattering model. According to [32], when $|\mathrm{I} - \mathrm{A}| \leq K$, the region is a bright area, and $J(x) = I(x)$. When $|\mathrm{I} - \mathrm{A}| \geq K$, the region satisfies the dark channel prior, the original transmission map remains unchanged, and the image is restored with (16), where K is the defined threshold. In contrast to [32], when $|\mathrm{I} - \mathrm{A}| \leq K$, the transmission is recalculated so that the $t(x)$ in the sky is more consistent with $t_{\text{real}}(x)$ and unified with the atmospheric scattering model. We redefine (14):

$$\underset{c \in \{R,G,B\}}{J^c}(x) = \frac{I^c - A^c}{\min\{\max\{\frac{K}{|I^c(x) - A|}, 1\} \bullet \max(t^c(x), t_0), 1\}} + A^c \tag{16}$$

The value of K is 50, which is the same as that in [32], and the sand-dust images corrected in (c) and (d) of Fig. 8 are shown in Fig. 9.

From Fig. 9, we can see that the color distortion in the sky is effectively addressed by improving the sky transmission map. However, there is still a color shift in the sand-dust image, so the color shift needs to be removed.

3.5 Recovery Model After Color Correction

From Fig. 9, we can see that the color distortion in the sky is effectively avoided by improving the sky transmission map. According to the histogram of the sand-dust image in Fig. 3, the relative position deviation of the three channels R, G, and B is large, and the pixel values of channels G and B are low, leading to a dark image. Based on the gray world algorithm [33] and the characteristics of the sand-dust histogram, the green and blue channels are adjusted according to the red channel,

(a) (b)

Fig. 10. Result of restoration after color correction. (a) Color correction result of Fig. 9(a). (b) Color correction result of Fig. 9(b).

TABLE 1
Pseudo-Code of Our Method

1. **Input:** Sand-dust image I.
2. Extract the R, G, and B channels of I and reverse the B channel.
3. Calculate the result of RBCP according to formula (10)
4. Use RBCP to estimate atmospheric light A.
5. Calculate transmittance t according to formula (12).
6. Improve t with guided filtering.
7. Apply formula (16).
8. Remove the color shift according to formula (18).
9. **Output:** Recovered image.

and the color gain adjustment factor is introduced.

$$\beta^c = \frac{\frac{1}{MN}\sum_{x=1}^{M}\sum_{y=1}^{N} I^r(x,y)}{\frac{1}{MN}\sum_{x=1}^{M}\sum_{y=1}^{N} I^c(x,y)} \tag{17}$$

where c represents the R, G and B channels and M and N are the length and width of the image, respectively. The numerator is the mean value of the red channel in the sand-dust image, and the denominator is the mean value of the three corresponding channels R, G and B. The color adjustment factor is introduced into (16), so the final model is:

$$\underset{c\in\{R,G,B\}}{J^c}(x) = \frac{\beta^c\left(I^c - A^c\right)}{\min\{\max\{\frac{K}{|I^c(x)-A|}, 1\} \bullet \max(t^c(x), t_0), 1\}} + \beta^c A^c \tag{18}$$

J is the final recovered sand-dust image. Fig. 10 is the result of restoration of Fig. 9 after color correction.

As shown in Fig. 10, the final color correction recovery model removes the color shift well and achieves good color fidelity. Here, we give the specific pseudo-code, as shown in Table 1.

4. Experimental Results

The pictures used in the experiment are real and nonsynthetic high-quality pictures from [19] and [37], and they are typical representatives of hazy images. In MATLAB 2016a, the host is configured on a computer with an Intel(R) Core(TM) i5-6500 CPU@3.2 GHz, an 8-GB memory and a 64-bit operating system to implement the algorithm of this article, and a large number of images were selected for experiments. The data of this algorithm are normalized. To verify the performance of

the proposed algorithm, this paper compares it with the methods proposed by Peng *et al.* [22], Ren *et al.* [27], Shin *et al.* [28], Ren *et al.* [30], Huang *et al.* [24], and Huang *et al.* [26] and provides quantitative and qualitative analyses. The experimental results are shown in Fig. 11.

4.1 Qualitative Evaluation

As seen from Fig. 11(b), the contrast of method [22] has been improved to a certain extent without removing the color shift; a reddish effect appears, which is caused by the inaccurate estimation of atmospheric light. [27] and [28] improve the visibility of the image, but they do not solve the color shift problem. In Image 4, the darkening of the top of the tower has been enhanced in [27]'s method, but the problem of color shift has not been solved. Fig. 11(e) shows that [30]'s method enhances the clarity of the image and has a good effect on distant scenery. From Image 2, we can see that the edges of the white roof in the distance are clearly visible. In Image 4, there is a slight halo. Due to overenhancement, the sky appears to be white to different degrees in the four images, but the color shift cannot be effectively removed. Fig. 11(f) shows that in the method of [26], the color shift is removed, and the clarity is poor; however, the foreground parts of Images 1 and 3 are more yellow because of the inaccuracy of the color correction model. Fig. 11(g) shows that although [24]'s method removes the color shift, the clarity is insufficient, and the sky shows a problem of blueness. This method adjusts color through the difference method of the color channel. For the sky region, because the mean value of the blue channel is low, the difference method causes blue distortion. Fig. 11(h) shows that, compared with other methods, the proposed method better reduces the color shift and has a better color fidelity effect. The clarity and contrast of the image have been greatly improved, and the overall visual effect is better. The reason is based on the characteristics of the sand-dust image spectrum. The proposed BRCP method can accurately estimate the transmission map and atmospheric light. In addition, the guided filtering and tolerance mechanism introduced in this paper improves transmittance and image visibility. Its color correction model is based on the gray world algorithm and combines the characteristics of the three channels of sand-dust images R, G, and B to achieve color correction, which removes the color shift well.

4.2 Quantitative Evaluation

In general, there are two broad categories of objective indicators of image restoration effects: reference methods and nonreference methods. In real scenes, it is unrealistic to expect to obtain an image without sand dust. Here, we use a nonreference method to evaluate the quality of image restoration. Two well-known quantification indexes e and r [34] are used to evaluate the restoration effect of each comparison method in a real scene. We also use the NBIQA index [35] to evaluate overall image quality. Specifically, e evaluates the comparative ease of discriminating the edge between the restored image and the original blurred image. r evaluates the average gradient before and after the restoration of blurred images to evaluate the average visibility. The larger the values of e and r are, the better the restored images are. NBIQA combines a large number of features in the spatial and transform domains based on natural scene information and comprehensively evaluates an image by predicting the image quality score. The higher the NBIQA score is, the higher the quality of the image. To evaluate the performance of the algorithms, the running time t is compared, and the evaluation index and performance comparison of their images are shown in Table 2.

In Table 2, the best results for indicators e, r and NBIQA are bolded. It can be seen from Table 2 that, compared with the six comparison algorithms, the indicators e and r are higher for our method than for other algorithms, which proves that the proposed method can recover more edges and achieve better visibility. From Fig. 11, we can see that our results have better visibility and more vivid colors. In particular, only in [30]'s method is the index r, in Image 2 and Image 4, higher than that in our method, which shows that [30]'s method has better contrast. On the other hand, we can see that there is an overenhancement phenomenon in [30]'s method. The NBIQA index is higher than it is for other algorithms. Only in [30]'s method is the NBIQA in Images 2 and 3 slightly

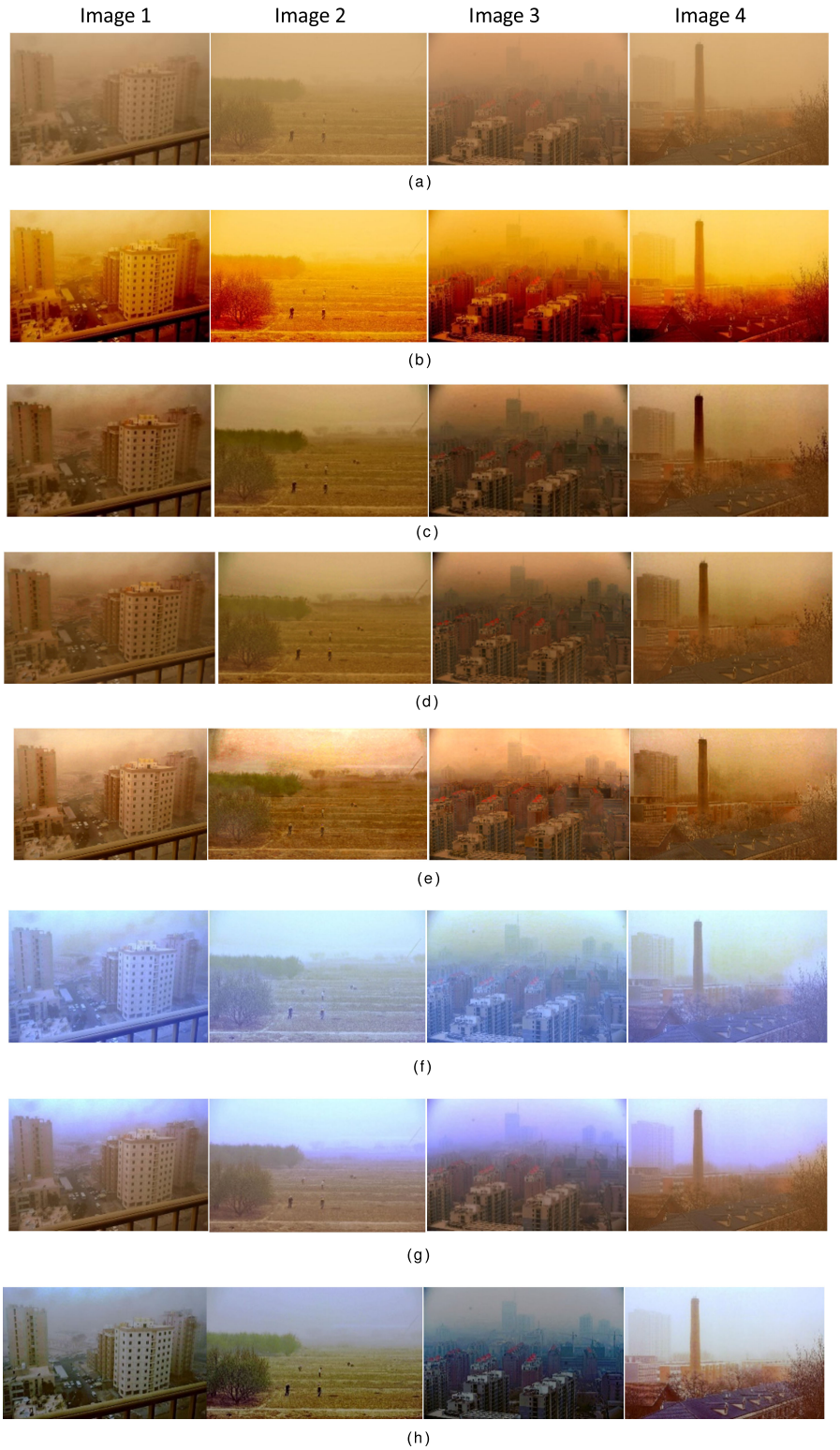

Fig. 11. Comparison results of the proposed algorithm and other algorithms. (a) Original sand–dust image. (b) The method of [22]. (c) The method of [27]. (d) The method of [28]. (e) The method of [30]. (f) The method of [26]. (g) The method of [24]. (h) The proposed method.

TABLE 2
The Evaluation Results of the Compared Methods by e, r, NBIQA and t

	Evaluation	[22]	[27]	[28]	[30]	[26]	[24]	Ours
Image1	e	0.6698	0.8970	0.8268	0.6451	0.5530	0.4695	**1.3011**
(600 x 400)	r	2.0096	1.6295	1.5273	1.6743	1.4586	1.3564	**2.7833**
	NBIQA	57.44	52.18	51.75	56.84	52.46	52.07	**62.26**
	t	0.70 s	2.02 s	3.82 s	5.64 s	3.03 s	0.75 s	1.29 s
Image2	e	5.2627	8.3761	6.1266	7.3775	7.4659	4.0177	8.7185
(950 x 586)	r	2.7103	2.0642	1.8191	**4.6517**	2.0824	1.6825	3.4274
	NBIQA	61.92	52.77	49.86	**71.44**	51.88	57.06	69.52
	t	0.92 s	4.38 s	7.29 s	6.82 s	6.85 s	1.68 s	3.06 s
Image3	e	0.4273	0.8650	1.0679	0.7260	0.5079	0.3841	**1.1143**
(900 x 600)	r	2.1181	1.4732	1.6454	1.7062	1.3543	1.1989	**2.4112**
	NBIQA	61.63	59.42	58.66	**69.83**	62.35	62.35	66.39
	t	0.88 s	3.74 s	6.81 s	6.16 s	6.68 s	1.53 s	2.79 s
Image4	e	0.5743	0.6679	0.9312	0.7093	0.5272	0.3865	**0.9814**
(940 x 626)	r	2.0875	1.4212	1.6184	**3.5022**	1.3961	1.2191	2.8390
	NBIQA	81.25	74.87	73.31	66.17	75.35	75.41	**85.51**
	t	0.96 s	4.12 s	7.83 s	6.41 s	7.13 s	1.66 s	3.32 s

higher than that for our algorithm. The reason is that the contrast of [30]'s method is relatively high, resulting in a higher evaluation score than our method. Based on these three indicators, the proposed algorithm is superior to comparative algorithms and has a better recovery effect and image quality. In terms of algorithm performance, we can see in Table 2 that the algorithm in [22] has the shortest running time and the best performance. The running time of our method is higher than that of the method in [24], ranking third among all the algorithms, which can meet the needs of real-time processing. Compared with other algorithms, the algorithms in [28], [30] and [26] have the longest running time. For small image sizes, the running time of our method is not very different from that of the methods in [22] and [24], as shown in Fig. 11, but our algorithm has the best effect in restoring sand-dust images.

4.3 Applications and Shortcomings of Our Algorithm

4.3.1 Application 1 Underwater Image Restoration: Considering that underwater images also have a color shift and low contrast, the algorithm proposed in this paper can be used for underwater image restoration. The effect is shown in Fig. 12.

From Fig. 12, the algorithm in this paper can effectively remove underwater color shifts and enhance the details of underwater images. It has a good effect on underwater images.

4.3.2 Application 2 Image Segmentation: The edges of sand-dust images are blurred, and there is a color shift in sand-dust images, which affects the accuracy of image segmentation. We use the mean shift proposed by [36] to segment a sand-dust image before and after enhancement, as shown in Fig. 13.

From Fig. 13, we can see that the enhanced sand-dust image can segment the ship's outline well. For sand-dust images, segmentation accuracy can be improved by using the algorithm.

Our method can be used for postprocessing of sand-dust video, and it can also help the image matching of sand-dust images. Due to the lack of related data sets, it will not be shown here.

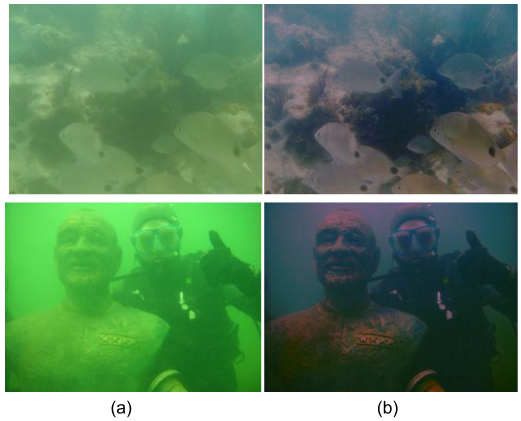

(a) (b)

Fig. 12. Results of underwater image restoration. (a) Original underwater image. (b) Results of restoration by our method.

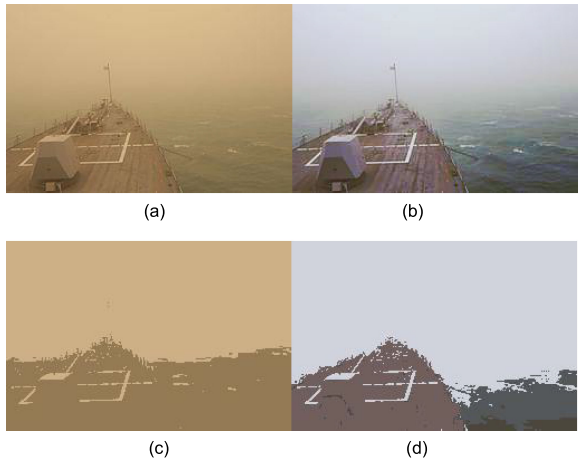

(a) (b)

(c) (d)

Fig. 13. Segmentation results of the mean shift. (a) Sand-dust image. (b) Enhanced result. (c) Segmentation result of (a). (d) Segmentation result of (b).

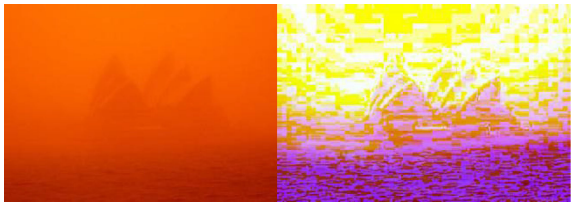

(a) (b)

Fig. 14. Example of failure. (a) Sand-dust image. (b) Result of restoration by our method.

4.3.3 Shortcomings of Our Algorithm: Our method cannot handle sand-dust images with a large degree of color shift, as shown in Fig. 14.

From Fig. 14, the effect of restoration by our method has serious color distortion. The sand-dust image restoration algorithm based on the atmospheric scattering model proposed cannot handle images with a large degree of sand-dust.

5. Conclusion

In this paper, we propose an effective method for sand-dust image restoration. The method is based on the atmospheric scattering model. With sand-dust particles, blue light is absorbed to a large degree so that the blue channel value of the image is relatively low, and a dark channel prior is not applicable to sand-dust image. RBCP is proposed. RBCP is used to estimate atmospheric light and transmission maps; then, the coarse transmission is improved by a guiding filter, and a tolerance method is used to improve the transmission map of bright sky areas to avoid distortion in the sky. This method effectively improves the clarity and contrast of the image. Finally, combined with the gray world, a color adjustment factor is introduced into the atmospheric scattering model to remove the color shift. The proposed method can effectively restore sand-dust images with good visibility and color fidelity. The experimental results show that the proposed method is superior to comparison algorithms through quantitative and qualitative analysis, and they demonstrate the superiority of the proposed algorithm.Our method can also restore the underwater image to some extent, and improve the accuracy of the sand-dust image segmentation, which proves the good applicability. In the future, we need to deal with serious degraded sand-dust images.

References

[1] R. Zhang, S. Newman, M. Ortolani, and S. Silvestri, "A network tomography approach for traffic monitoring in smart cities," *IEEE Trans. Intell. Transp. Syst.*, vol. 19, no. 7, pp. 2268–2278, Jul. 2018.

[2] B. Irani, J. Wang, and W. Chen, "A localizability constraint-based path planning method for autonomous vehicles," *IEEE Trans. Intell. Transp. Syst.*, vol. 20, no. 7, pp. 2593–2604, Jul. 2019.

[3] A. Elliethy and G. Sharma, "Vehicle tracking in wide area motion imagery via stochastic progressive association across multiple frames," *IEEE Trans. Image Process.*, vol. 27, no. 7, pp. 3644–3656, Jul. 2018.

[4] E. J. Mccartney and F. F. Hall Jr., *Optics of the Atmosphere: Scattering by Molecules and Particles*, New York, NY, USA: John Wiley and Sons, Inc., 1976, p. 421.

[5] F. Gasparini and R. Schettini, "Color correction for digital photographs," in *Proc. - 12th Int. Conf. Image Anal. Process.*, 2003, pp. 646–651.

[6] K. Iqbal, M. Odetayo, A. James, R. A. Salam, and A. Z. H. Talib, "Enhancing the low quality images using unsupervised colour correction method," in *Proc. Conf. - IEEE Int. Conf. Syst. Man Cybern.*, 2010, pp. 1703–1709.

[7] C. Liu, X. Chen, and Y. Wu, "Modified grey world method to detect and restore colour cast images," *IET Image Process.*, vol. 13, no. 7, pp. 1090–1096, May 2019.

[8] E. Zhang, Y. Zhang, and J. Duan, "Color inverse halftoning method with the correlation of multi-color components based on extreme learning machine," *Appl. Sci.*, vol. 9, no. 5, pp. 841–852, 2019.

[9] M. Afifi, B. Price, S. Cohen, and M. S. Brown, "Supplemental material for when color constancy goes wrong: Correcting improperly white-balanced images," in *Proc. Conf. Comput. Vision Pattern Recognit.*, 2019, pp. 1535–1544.

[10] G. Narasimhan, S. Nayar, and K. Shree, "Vision and the atmosphere," *Int. J. Comput. Vis.*, vol. 48, no. 3, pp. 233–254, 2002.

[11] S. G. Narasimhan and S. K. Nayar, "Contrast restoration of weather degraded images," *IEEE Trans. Pattern Anal. Mach. Intell.*, vol. 25, no. 6, pp. 713–724, Jun. 2003.

[12] J. P. Tarel and N. Hautière, "Fast visibility restoration from a single color or gray level image," in *Proc. IEEE Int. Conf. Comput. Vision*, 2009, pp. 2201–2208.

[13] R. Fattal, "Single image dehazing," *Assoc. Comput. Machinery Trans. Graph.*, vol. 27, no. 3, pp. 1–9, 2008.

[14] K. He, J. Sun, and X. Tang, "Single image haze removal using dark channel prior," *IEEE Trans. Pattern Anal. Mach. Intell.*, vol. 33, no. 12, pp. 2341–2353, Dec. 2011.

[15] J. Zhang and D. Tao, "FAMED-Net: A fast and accurate multi-scale end-to-end dehazing network," *IEEE Trans. Image Process.*, vol. 29, no. 1, pp. 72–84, Apr. 2019.

[16] A. Dudhane and S. Murala, "RYF-Net: Deep fusion network for single image haze removal," *IEEE Trans. Image Process.*, vol. 29, pp. 628–640, Aug. 2019.

[17] B. Li, X. Peng, Z. Wang, J. Xu, and D. Feng, "AOD-Net: All-in-One dehazing network," in *Proc. IEEE Int. Conf. Comput. Vis.* 2017, pp. 4780–4788,.

[18] A. Wang, W. Wang, J. Liu, and N. Gu, "AIPNet: Image-to-Image single image dehazing with atmospheric illumination prior," *IEEE Trans. Image Process.*, vol. 28, no. 1, pp. 381–393, Jan. 2019.

[19] X. Fu, Y. Huang, D. Zeng, X.-P. Zhang, and X. Ding, "A fusion-based enhancing approach for single sandstorm image," in *Proc. IEEE 16th Int. Workshop Multimedia Signal Process.*, 2014, pp. 1–5.

[20] T. Yan, L. Wang, and J. Wang, "Method to enhance degraded image in dust environment," *J. Softw.*, vol. 9, no. 10, pp. 2672–2677, Oct. 2014.

[21] S. Yu, Z. Hong, W. Jing, Z. Fu, X. Shan, and S. Hua, "Single sand-dust image restoration using information loss constraint," *Opt. Acta Int. J. Opt.*, vol. 63, no. 21, pp. 2121–2130, 2016.

[22] Y.-T. Peng and P. C. Cosman, "Single image restoration using scene ambient light differential," in *Proc. IEEE Int. Conf. Imag.Process.*, Sep. 2016, pp. 1953–1957.

[23] Y.-T. Peng, K. Cao, and P. C. Cosman, "Generalization of the dark channel prior for single image restoration," *IEEE Trans. Image Process.*, vol. 27, no. 6, pp. 2856–2868, Jun. 2018.
[24] S.-C. Huang, B.-H. Chen, and W.-J. Wang, "Visibility restoration of single hazy images captured in real-world weather conditions," *IEEE Trans. Circuits Syst. Video Technol.*, vol. 24, no. 10, pp. 1814–1824, Oct. 2014.
[25] S. C. Huang, J. H. Ye, and B. H. Chen, "An advanced single-image visibility restoration algorithm for real-world hazy scenes," *IEEE Trans. Ind. Electron.*, vol. 62, no. 5, pp. 2962–2972, May 2015.
[26] S.-C. Huang, B.-H. Chen, and Y.-J. Cheng, "An efficient visibility enhancement algorithm for road scenes captured by intelligent transportation systems," *IEEE Trans. Intell. Transp. Syst.*, vol. 15, no. 5, pp. 2321–2332, Oct. 2014.
[27] W. Ren, L. Si, Z. Hua, J. Pan, X. Cao, and M. H. Yang, "Single image dehazing via multi-scale convolutional neural networks," in *Proc. IEEE Comput. Soc. Conf. Comput. Vis. Pattern Recognit.*, 2016, pp. 154–169.
[28] J. Shin, M. Kim, J. Paik, and S. Lee, "Radiance-Reflectance combined optimization and structure-guided ℓ_0-Norm for single image dehazing," *IEEE Trans. Multimedia.*, vol. 22, no. 1, pp. 1–16, Jan. 2019.
[29] Z. Shi, Y. Feng, M. Zhao, E. Zhang, and L. He, "Let you see in sand dust weather: A method based on halo-reduced dark channel prior dehazing for sand-dust image enhancement," *IEEE Access*, vol. 7, pp. 116722–116733, 2019.
[30] W. Ren *et al.*, "Gated fusion network for single image dehazing," in *Proc. IEEE Comput. Soc. Conf. Comput. Vis. Pattern Recognit.*, pp. 3253–3261, 2018.
[31] K. He, J. Sun, and X. Tang, "Guided image filtering," *IEEE Trans. Pattern Anal. Mach. Intell.*, vol. 35, no. 6, pp. 1397–1409, Jun. 2013.
[32] H. Xu, J. Guo, Q. Liu, and L. Ye, "Fast image dehazing using improved dark channel prior," in *Proc. IEEE Int. Conf. Inf. Sci. Technol.*, 2012, pp. 663–667.
[33] A. Hurlbert, "Formal connections between lightness algorithms," *J. Opt. Soc. Am. A Opt. Image Sci.*, vol. 3, no. 10, pp. 1684–1693, 1986.
[34] N. Hautiere, J. P. Tarel, D. Aubert, and E. Dumont, "Blind contrast enhancement assessment by gradient ratioing at visible edges," *Image Anal. Stereology*, vol. 27, no. 2, pp. 87–95, 2011.
[35] F. Ou and Y. Wang, "A novel blind image quality assessment method based on refined natural scene statistics," in *Proc. IEEE Int. Conf. Image Process.*, 2019, pp. 1004–1008.
[36] D. Comaniciu and P. Meer, "Mean shift: A robust approach toward feature space analysis," *IEEE Trans. Pattern Anal. Mach. Intell.*, vol. 24, no. 5, pp. 603–619, May 2002.
[37] 2019. [Online]. Available: https://image.baidu.com